Author's Accepted Manuscript

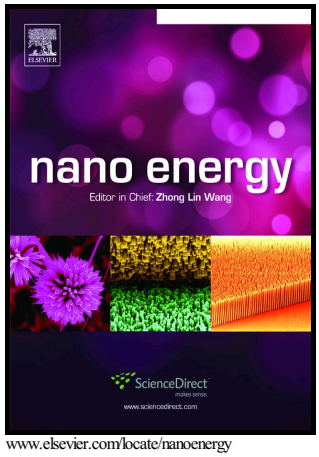

www.elsevier.com/locate/nanoenergy

Upper Limits for Output Performance of Contact-Mode Triboelectric Nanogenerator Systems

Bao Yang, Xiao-ming Tao, Ze-hua Peng

PII: Sxxxx
DOI: https://oi.org/10.1016/.nanoen.2018.12.013
Reference: NANOENxxxx

To appear in: *Nano Energy*

Received date: 11 September 2018
Revised date: 8 November 2018
Accepted date: 6 December 2018

Cite this article as: Bao Yang, Xiao-ming Tao and Ze-hua Peng, Upper Limits for Output Performance of Contact-Mode Triboelectric Nanogenerator Systems, *Nano Energy,* https://doi.org/10.1016/j.nanoen.2018.12.013

Upper Limits for Output Performance of Contact-Mode Triboelectric Nanogenerator Systems

Bao Yang[a], Xiao-ming Tao[a*], Ze-hua Peng[a,b]

[a] Nanotechnology Center of Functional and Intelligent Textiles and Apparel, Institute of Textiles and Clothing, The Hong Kong Polytechnic University, Hong Kong

[b] School of Energy and Environment, City University of Hong Kong, Hong Kong

*Corresponding author. xiao-ming.tao@polyu.edu.hk

Abstract

Intensive research efforts have been devoted to increasing output performance of triboelectric nanogenerators (TENGs) by selecting or modifying materials, increasing effective area, optimizing device structures and harvesting circuits. Considering field emission and gas-ionization for electric breakdown, this paper proposes new theoretical models to predict the upper limits for output performance of contact-mode TENG harvesting system. It reveals that a constant surface charge density exists on the dielectric layer with an effective thickness below a critical value. The resultant TENG exhibits a high output power. The working efficiency of the TENG harvesting system quantitatively highlights the scope and focus of improvement for high output power. The findings would provide a powerful tool to guide the experimental design in selection of materials, structure of TENG, harvesting circuits and storage device for intended applications.

Graphical abstract

fx1

Keywords:

triboelectric nanogenerators, high performance, upper limit, working efficiency, paper-based electronic devices, energy harvester

1. Introduction

Intensive research efforts have been devoted to powering trillions of microelectronics devices and systems, while minimizing environmental impact and providing user convenience. Triboelectric nanogenerators (TENGs), scavenging mechanical energy from our living environment by coupling of triboelectrification and electrostatic induction effects, have been demonstrated their potentials for a wide range of applications, such as self-powered sensors, wearable electronic systems, and power sources [1-9]. Up to data, the time-average output power from wearable TENG systems has reached microwatts, still several orders of magnitude away from most real applications of wearable microelectronic systems, which are typically driven by electric power in milliwatts. Hence, enhancement of output power is extremely crucial for the intended application of TENGs. One would naturally ask how much further improvement can be made, to milliwatt or even higher? What is the theoretical upper limit of outputs from a given TENG and operational conditions?

The materials, structures of devices, harvesting circuits and operation conditions will affect the actual output power of TENGs. Among these influencing factors, the effective surface charge density on the dielectric layer is the single most important one that has a quadratic (the highest order) effect on the output power [10-12]. Thus, various efforts have been devoted to obtaining high effective surface charge density by selecting materials in triboelectric series [13], increasing reactive area [14, 15], modifying materials [16], and imparting more charges on the surface of the dielectric layer by ionized-air injection [17]. The high surface charge density generates a strong electric field in the surrounding media (such as air). When the strong field reaches to a threshold value, electric breakdown will occur due to gas-ionization [18]. From Paschen's law for electric breakdown, a theoretical model was constructed to predict the maximum surface charge density on the dielectric layer, an agreement was reported between theoretical and experimental results of FEP films with a thickness of 50 -120 μm [17]. These results make an important step forward to determine the maximum surface charge density for TENG.

However, such a theoretical treatment derived from Paschen's law may be invalid when the calculated charge density become negative or infinitely large at a very small separation distance. In a contact-mode TENG, the electric breakdown behavior at a small gap distance is significantly important because the charge density on the interactive surfaces reaches the highest level at just beginning of the separation during

the whole working cycle. Moreover, the field emission [19, 20] due to the high electric field may dominate the breakdown then. Previous experimental evidences show that the breakdown voltage of gas in a microscale gap, from hundreds of nanometers to several microns, is drastically deviated from those predicted by the Paschen's law [19-22]. This filed-emission induced breakdown will result in variation in the surface charge density as well as the outputs of TENGs. Therefore, it is highly desirable to investigate this phenomenon and its influences on TENG.

Incorporating the electric breakdown mechanisms of induced field emission and gas-ionization, this work proposes a new theoretical model to predict the upper limit of surface charge density for contact-mode TENGs. From this, the upper limits of the transferred charge and output power of a contact-mode TENG harvesting system are presented. The working efficiency of a TENG harvesting system is defined as a product of individual efficiencies, associated with the TENG, its harvesting circuits and storage devices, respectively. A case study illustrates the scope and ways of further improvement on the actual output performance of a contact-mode TENG harvesting system.

2. Upper Limit of Charge Density on Dielectric Surface

Surface charge density on the dielectric layer is the most important influential factor on output power as mentioned above. Electric breakdown of air following the Paschen's law has been demonstrated to be the limiting condition of surface charge

[17, 23]. However, the important breakdown behavior between closely spaced contact has not been investigated carefully, whose breakdown voltage are much smaller than those described by the Paschen law [19-22]. By comprehensive comparison, as shown in **Supporting Information S1**, a modified model for the breakdown voltage of gas, V_b, across a small gap, incorporating the field emission and gas-ionization, is chosen in the following simple and explicit expression.

$$V_b = \begin{cases} Kx, & \text{for } 0 < x \le x_c \\ \dfrac{Bpx}{\ln(px) + C}, & \text{for } x_c \le x \le x_{\max} \end{cases} \quad (1)$$

where K is the threshold electric field required for field emission, which is discussed carefully in the **Supporting Information S1**. $C = \ln[A/\ln(1+1/\gamma)]$, p is the gas pressure, γ is the secondary ionization coefficient, A and B are constants determined by the composition and the pressure of gas. x_{max} is the max separation distance between interactive surfaces in TENGs. A critical value, x_c, determined by the interception point of the piecewise function, divides the gap distance into two regions. As shown in **Figure 1c**, when x is less than x_c, defined as pre-x_c region, a low breakdown voltage is dominated by field emission, and when x is larger than x_c, defined as post-x_c region, the breakdown voltage is dominated by gas-ionization following the Paschen's law. It is noted that without specification, all the parameters utilized in calculation or simulation are listed in **Table 1**.

The study of maximum surface charge for triboelectric nanogenerator [17] has been demonstrated that the Paschen's law is valid for electric contact between metal

electrode and charged polymer, by using ion-injection FEP films. Moreover, a lower threshold field emission (about 4 V/μm) of non-conjugated polymer coated on molybdenum or niobium cathode was obtained, which is 2.5-3 times lower than those from the cathodes without coating [24]. Therefore, the field emission from the effective cathode, such as the surface of polymer coating accumulated negative charges, may be an important influential factor on the maximum surface charge density. This proposed model of V_b, using the mechanisms of field emission and gas-breakdown, describes the upper limit of the working voltage across the gap from zero to a given distance. As shown in **Figure S1**, this proposed model at most of regions are consistent with those of the previous model[19], excepting the values of the points (near x_c), defined as transition regions from pure field emission to gas breakdown, are slightly higher. The working voltage across the gap of the TENG is normally lower than V_b predicted by different models in the region (near x_c), due to the reduction of charges that are transferred from the interactive electrode (electrode 1) to the bottom electrode (electrode 2), making a lower working voltage. Thus, the values at the points (near x_c) do not affect the prediction of output performance. It is reasonable to assume that the proposed model of V_b can be applied in TENGs.

The voltage across the gap, V_g, in TENGs is never larger than V_b due to the limitation of electric breakdown. As shown in **Figure 1a** and **1b**, a dielectric-conductor TENG, which has advantages of high structural figure-of-merits [25] and ease of integration, is used to illustrate the influence of electric breakdown on the upper limit of surface

charge density in a holistic manner. Apart from triboelectric surface, the top surface of the dielectric layer plays another role of cathodes for the effective capacitors across the gap and the dielectric layer, respectively. Based on the principle of charge conservation, the surface charge density on the dielectric layer is comprising by two parts: one is equal to surface charge density on electrode 1, σ_1, limited by electric breakdown in the gap, and the other is equal to surface charge density on electrode 2, σ_2, limited by the transferred charge between electrodes, neglecting electric breakdown in the dielectric layer due to its ultrahigh breakdown voltage which cannot be reached in TENGs. From theoretical derivation shown in the **Supporting information S2 and S3,** the highest surface charge density, σ_b, can be obtained theoretically when the TENG works at the breakdown voltage and most transferred charge on electrode 2, which implies that the TENG is under the short circuit condition. To avoid electric breakdown, the surface charge density should satisfy the relationship of $\sigma < \sigma_b$ at any $x > 0$, making V_g is always lower than V_b. Thus, the upper limit of surface charge density, σ_{UL}, that is the maximum value, can be given by

$$\sigma_{UL} = \min(\sigma_b) \tag{2}$$

where $\sigma_b = \begin{cases} K\varepsilon_0 \dfrac{d_0 + x}{d_0}, & \text{for } 0 < x \le x_c \\ \dfrac{Bp\varepsilon_0}{\ln(px) + C} \dfrac{d_0 + x}{d_0}, & \text{for } x_c \le x \le x_{\max} \end{cases}$, ε_0 is the permittivity of vacuum, and x is the separation distance, and d_0 represents the effective thickness of the dielectric layer, which is defined as the ratio of the thickness, d, and the relative permittivity, ε_r.

The breakdown behavior determined by field emission at a very small separation distance, only possessing tenths or hundredths of the whole separation, makes a significant influence on the upper limit of surface charge density. Because the charge density on interactive surfaces at the beginning of separation is limited by the ability of charge-generation and the electric breakdown induced by field emission, reflecting and determining its highest achievable level during the whole working cycle of TENGs.

Other two influential factors of d_0 and x make an eminent influence on the transferred charge between electrodes, inducing a different theoretical upper limit of surface charge density without electric breakdown. For a thick dielectric layer, such as 20 μm in d_0, the upper limit of surface charge density, $\sigma_{UL,}$ of 308 μC/m^2 (red) is consistent with that predicted (blue) by the previous model [17], as shown in **Figure 1d**. With descending effective thickness from 20 to 2 μm, σ_{UL} of 513 μC/m^2 (red) is significantly lower than 1615 μC/m^2 (blue), as shown in **Figure 1e**. Meanwhile, x_{max} is normally several millimeters or higher in TENGs, which is two or higher orders larger than the spacing, where the electric breakdown limits σ_{UL}. Thus, the influence of x_{max} can be neglected. The numerical plot of σ_{UL} against d_0 with different K (**Figure 1f**) illustrates that a critical thickness, d_c, divides the curves into two regions. σ_{UL} is normally larger at a smaller d_0 in the post-d_c region, and σ_{UL} is constant in the pre-d_c region. A higher σ_{UL} in a narrower pre-d_c region is obtained with a higher K.

Moreover, σ_{UL} in the pre-d_c region, $\sigma_{UL\_pre\text{-}dc}$, has a linear dependence on K, as shown in **Figure 1g**. The evaluation of d_c is provided in **Supporting Information S4**, which reveals that d_c has a repaid reduction when K increases, as shown in **Figure 1h**. A higher surface charge density, possessing higher output power, is normally obtained at a thinner dielectric layer. Even electric breakdown dominated by field emission at a very small gap distance, K plays an important role on the upper limit of surface charge density when the thickness of the dielectric layer decreases into pre-d_c region. Therefore, increasing of K and decreasing of d_0 will be an effective way to enhance the surface charge density and the possessing output power of the TENG.

3. Upper Limit of Transferred Charge Between Electrodes

Output performance of a TENG harvesting system relies on two components associated with the TENG and its harvesting circuits, respectively. Surface charge density on the dielectric layer reflects the potential of output, while the transferred charge between electrodes is a more direct and comprehensive indicator for the outputs of TENG harvesting systems, especially for its harvesting circuits. The upper limit of surface charge density on the dielectric layer has been studied above, where no electric breakdown occurs in the gap. Thus, the transferred charge, Q, in TENGs follows the previous model [10].

$$Q = \frac{S\sigma_{UL}x}{d_0 + x} \tag{3}$$

where σ has been replaced by σ_{UL}, and S is area of the interactive surface. Apart from

decreasing surface charge density, a lower d_0 is another effectively way to bring down V_g by inducing more transferred charge to avoid electric breakdown, shown in equation (S2-7).

With a high charge density (up to $K\varepsilon_0$, limited by field emission) on the dielectric layer at different d_0, three cases of V_g may occur, as shown in **Figure 2a**. First, if a thick dielectric layer (such as 20 μm in d_0, at the post-d_c region) is utilized, a rapidly increasing curve of V_g (the red curve with circles) will contact the part of V_b defined by Paschen's law, marked as case 1. If a very thin dielectric layer (such as 5 μm in d_0, at the pre-d_c region) is utilized, a slowly increasing curve of V_g (the red curve with triangles) never reaches V_b, in other word, no gas breakdown occurs, marked as case 3. Between case 1 and case 3, there is a case that the curve of V_g (the red curve with stars) tangentially contacts V_b at one point, marked as case 2, where the thickness of the dielectric layer is 8.7 μm at d_c. Since gas breakdown occurs, Q in case 1 will be more complex than those in case 2 and 3. Based on the assumption that TENGs can work very close to the breakdown voltage, the derivation of σ, Q and V_g for case 1 with three regions of before, during, and after gas breakdown are given by equation (S5-19), (S5-20) and (S5-21), respectively. The details are given in **Supporting Information S5**. As shown in **Figure 2b**, σ of case 1 in the region before electric breakdown is the same as that of case 2 and 3, then reduces within the region of electric breakdown and becomes constant after electric breakdown, meanwhile, σ in case 2 and 3 is the same as a constant.

The transferred charge at x_{max}, $Q(x=x_{max})$, in case 2 and 3 are similar, which is higher than that in case 1, as shown in **Figure 2c**. When the separation distance is more than 1 mm, the transferred charge tends to be constant. Enlarged plot of Q shown in **Figure 2d** indicates that a rapider increasement of Q is normally obtained at a smaller d_0. For a given K, as shown in **Figure 2e**, d_c divides d_0 into two regions: a higher $Q(x=x_{max})$ is normally obtained at a smaller d_0 in post- d_c region, and $Q(x=x_{max})$ tends to be constant at the pre-d_c region, reflecting the upper limit, defined as Q_{UL}. Moreover, the equation (3) also clearly reveals that Q_{UL} is obtained at a very small d_0 with x_{max}. Since x_{max} is several orders larger than such d_0, combining equation (2) or **Figure 1f**, Q_{UL} can be easily evaluated by

$$Q_{UL} = SK\varepsilon_0 \tag{4}$$

Thus, there is a linear relationship between Q_{UL} and K, as shown in **Figure 2f**.

4. Upper Limit of Output Power and Working Efficiency of TENG

A TENG harvesting system comprise a TENG, harvesting circuits and a storage device, where the TENG supplies charges, and harvesting circuits pump the charges into the storage device. Thus, an ideal TENG harvesting system with a 100% working efficiency implies that all the electric charges, that is, the upper limit of the transferred charge, should be pumped into the storage device without any loss. From equation (4), the upper limit outputs of voltage, V_{UL}, and power, P_{UL}, of an ideal harvesting system after n cycles are derived in **Supporting Information S6**. V_{UL} is proportional to the

harvesting cycles of n and $Q_{UL,}$ and is negatively proportional to the capacitance, C_L, of an ideal storage element, as shown in equation (S6-1). Moreover, equation (S6-3) clearly reveals that Q_{UL} has a quadratic effect on P_{UL}, while n, f, and C_L has a linear effect. Since Q_{UL} is proportional to K, P_{UL} also shows a quadratic dependence on K, as shown in equation (S6-4).

In practice, a real TENG harvesting system does not satisfy all the above assumptions due to the limitations in structures, materials, harvesting circuits and storage devices. Comparing to the output power of the ideal system, the working efficiency, η, can quantitatively determine the potential and current level of achievement as well as highlight the scope of improvement for high output power of an actual system. It is given by

$$\eta = \frac{P_e}{P_{UL}} \tag{5}$$

where P_e is the actual output power of a TENG harvesting system after n cycles, which is calculated by $P_e = \frac{V_L^2 C_L f}{2n}$, where V_L is the measured voltage and f is the working frequency of the TENG. η varies from 1 to 0, representing that all the charge (Q_{UL} at each half cycle) to zero charge bumped into the storage element. η can be also expressed by a product of two items: $\eta_1 = \left(\frac{Q_e}{Q_{UL}} \right)^2$ as the efficiency of the TENG device, and $\eta_2 = \frac{\eta}{\eta_1}$ as the efficiency of the harvesting circuit and storage devices. Q_e obtained experimentally is the transferred charge during the releasing-half

cycle.

5. Case Study of Contact-mode TENG Harvesting System

In studying the field-emission-induced electric breakdown, the threshold electric field, *K*, is approximately proportional to the work function and reversely proportional to the field enhancement factor due to surface irregularities, as shown in equation (S1-6). The work function of polymers normally falls in a small range of several electronvolt [26], such as PTFE (5.75 eV), PE (4.90 eV) and Nylon-66 (4.30 eV). The field enhancement factor is typically from 140 to 247 [27] for even contacts between polished metals. Thus, the field enhancement factor associated with surface irregularities may exert a more significant influence on *K*, meaning smooth surfaces or well matching interactive surface is desirable for a higher *K*. Increasing surface roughness or micro-patterns plays dual roles of enhancement of surface area and uplift of the electric-field enhancement factor. The first role may increase the actual contact area, making more tribo-charge and having a high output performance. The other role decreases the threshold value of field emission, inducing electric breakdown is easier to happen and having a dramatic reduction on the surface charge density. There is a completive relationship between these two roles. When surface charge density is low, where the electric field generated by surface charge is not enough strong to induce field emission, the influence of the enhancement of the electric-field enhancement factor on the surface charge density can be neglected. Thus, increasing surface roughness or micro-patterns can have a positive effective on the enhancement of output performance. However, if the surface charge density is already high, where the generated electric field is close to the threshold of field emission, the influence of the enhancement of the electric-field enhancement factor on the surface charge will be great. When electric breakdown induced by field emission happens, the surface charge and the possessing outputs will drastically decrease. Increasing surface

roughness or micro-patterns will have a negative effective. Therefore, the surface profile of the dielectric layer should be controlled for similar or same contacts.

Schematic diagram of a laboratory-fabricated contact-mode TENG is shown in **Figure 3a**, which is light weight, safe and non-toxic, robust in repeated deformation. The harvesting system is shown in **Figure 1b**. Polydimethylsiloxane (PDMS) was chosen as the electronegative dielectric material due to its characteristics of high affinity to attract electrons, flexibility, durability, and more importantly, easy to make a smooth surface by coating. After a comparison study among various electrodes, shown in **Supporting Information S7**, Cu/Ni coated aramid paper (Type of L843/45, provided by LongPont Co. Ltd, China) was selected as the flexible electrodes due to its high strength, light weight, a wide range of working temperature, good recovery, good conductivity, fatigue resistance and high output voltage. A scanning electron microscopy (SEM) of the Cu/Ni coated aramid paper in **Figure 3b** indicates that the surface has microscale irregularities due to the raised fibers and voids between the fibers. To obtain a smooth surface, PDMS was coated on the conductive aramid paper layer-by-layer by using an automatic coating machine (MSK-AFA-III). The surface profiles of the Cu/Ni coated aramid paper and PDMS coating are illustrated in **Figure 3c and 3d**, respectively, measured by an optical measurement system (ZeGage^{TM} Plus 3D Optical Surface Profiler with sub-nanometer Precision). The surface roughness is 1.81 and 0.61 μm in the arithmetical mean height, S_a, respectively. More PDMS coating surfaces, as shown in **Figure S4,** demonstrate similar profiles as expected.

Moreover, the surface of PDMS coating tends to follow the surface profile of the conductive aramid paper, since the modulus of the conductive aramid paper is several orders higher than that of PDMS. During all tests, the same aramid conductive paper was utilized as electrode 1. Therefore, it is reasonable to consider that the PDMS coatings have a similar surface roughness. The relative permittivity of PDMS coating is about 3.4 below 1000 Hz, measured by a precision impedance analyzer (Agilent 4294A). The fabricated TENG with the nominal interactive surface of 6×6 cm^2 was compressed by a Keyboard Life Tester (ZX A-03), which provides a continuous sinusoidal motion [12]. As shown in **Figure 3e**, the output voltage was monitored by an oscilloscope (DSO-X3014A) via a differential voltage probe (N2790A), where the effective resistance is 8 MΩ. After 1,000,000 cycles, the peak-peak voltage of about 500 V, twice as the previous output voltage [12], does not show any degradation, indicating that the fabricated TENG has an excellent durability. Electric sparks were found during the releasing-half cycle when the fabricated TENG connected with a resistance, such as 8 MΩ, as shown in **Supporting Information: Movie 1**.

After a sufficient number of contacts, more than 5000 cycles, the fabricated TENG was connected to a capacitor (100 μF) via a full-bridge rectifier shown in **Figure 1b**. **Figure 4a** depicts an excellent agreement between experimental and theoretical results predicted by the model [11] when the number of cycles is less than 1000. With ascending compress cycles, where *n* is more than 2000 cycles, the measured voltage increases. However, it is lower than that predicted due to the main factor of large

leakage current of the actual capacitor and diodes, and possible electric breakdown. When the applied voltage is over a threshold, the leakage current of capacitor and diodes will drastically increase from a neglectable level to an ultrahigh level. Moreover, when the applied voltage across the capacitor is high, the working voltage across the gap also increases, described by equation (S2-4), inducing that electric breakdown is more possible to happen. Thus, when n is below 1000 cycles or V_L is below 18 V in this harvesting circuit, the leakage current of the capacitor and diodes appears very small and can be neglected, the achievable or the upper limit of surface charge density in the fabricated TENG can be predicted by the model [11]. The derivation is shown in **Supporting Information S9**.

Figure 4b and **4c** demonstrate that a higher V_L or P_e is normally obtained with a smaller d_0. The corresponding surface charge density illustrated in **Figure 1f** reveals that all σ are lower than those predicted by the model from Paschen's law [17], and σ tends to be a constant when d_0 is below d_c of 32 μm. When d_0 = 58 μm in the post-d_c region, gas-breakdown occurs during the working cycle, the surface charge density is lower than the predicted σ_{UL} because of random electric behavior. If the threshold value, K, for field emission is estimated as 27 MV/m, as shown in **Supporting Information S9**, an excellent agreement between theoretical and experimental results of the effective surface charge density is obtained at the investigated range from 7 to 28 μm in d_0.

For the TENG harvesting system illustrated in **Figure 1b**, the working efficiency, η, depends on d_0 and n. A higher efficiency is normally obtained with a smaller d_0, as shown in **Figure 4d**. When d_0 increases from 7 to 58 μm, η decreases from unity to 0.35. **Figure 4e** reveals the relationship between η and n. A rapid reduction of η occurs when n is more than 1000 cycle, which may be due to the fast-increased leakage current of the harvest circuits or storage devices in the system. These results show solid evidences for the design of multilevel storage. Before the working efficient has an obvious reduction, such as below 1000 cycles, the charge in the capacitor should be pumped into another storage element at higher level, avoiding loss induced by the leakage current and electric breakdown.

5. Conclusion

Incorporating the electric breakdown due to field-emission and gas-ionization of gas, we have proposed new theoretical models for the upper limits of surface charge density, transferred charge, and output power of contact-mode TENG harvesting systems, respectively. The breakdown is considered in two regions divided by a critical effective thickness (d_c) of the dielectric layer. In the pre-d_c region, due to the dominating field-emission induced breakdown, the upper limit of surface charge density is constant, which is significantly lower than that predicted by the previous model from Paschen's law. A small effective thickness of the dielectric layer below d_c can result in more transferred charges (close to the upper limit) and a high output power. The working efficiency of the harvesting system is defined to quantitatively

highlight the scope of improvement for high output power. A case study on the TENG harvesting system reveals that the upper limit of surface charge density at the pre-d_c region is constant as expected, and a higher working efficiency is obtained at a smaller effective thickness of dielectric layer and less working cycle. These results offer an important insight for the design of TENG harvesting systems in selection of materials, structure of TENG devices, harvesting circuits and energy storage devices.

Acknowledgements

The authors wish to acknowledge funding support from Research Grants Council (Project No. 525113, 15215214, 15211016, 15200917), and Innovation and Technology Commission (Project No. ITP/039/16TP) of Hong Kong SAR Government.

Video caption: " Occurrence of electric sparks in a contact-mode TENG"

Reference

[1] Z.L. Wang, L. Lin, J. Chen, S. Niu, Y. Zi, Triboelectric Nanogenerators, Springer 2016.

[2] S. Chen, X.M. Tao, W. Zeng, B. Yang, S.M. Shang, Quantifying Energy Harvested from Contact-Mode Hybrid Nanogenerators with Cascaded Piezoelectric and Triboelectric Units, Adv. Energy. Mater. 7(5) (2017). https://doi.org/10.1002/aenm.201601569

[3] J. Song, B. Yang, W. Zeng, Z. Peng, S. Lin, J. Li, X. Tao, Highly Flexible, Large-Area, and Facile Textile- Based Hybrid Nanogenerator with Cascaded Piezoelectric and Triboelectric Units for Mechanical Energy Harvesting, Adv. Mater. Technol.

(2018) 1800016. https://doi.org/10.1002/admt.201800016

[4] G. Zhu, P. Bai, J. Chen, Z.L. Wang, Power-generating shoe insole based on triboelectric nanogenerators for self-powered consumer electronics, Nano Energy 2(5) (2013) 688-692. https://doi.org/10.1016/j.nanoen.2013.08.002

[5] S.M. Niu, Z.L. Wang, Theoretical systems of triboelectric nanogenerators, Nano Energy 14 (2015) 161-192. https://doi.org/10.1016/j.nanoen.2014.11.034

[6] G. Zhu, B. Peng, J. Chen, Q.S. Jing, Z.L. Wang, Triboelectric nanogenerators as a new energy technology: From fundamentals, devices, to applications, Nano Energy 14 (2015) 126-138. https://doi.org/10.1016/j.nanoen.2014.11.050

[7] H.J. Choi, J.H. Lee, J. Jun, T.Y. Kim, S.W. Kim, H. Lee, High-performance triboelectric nanogenerators with artificially well-tailored interlocked interfaces, Nano Energy 27 (2016) 595-601. https://doi.org/10.1016/j.nanoen.2016.08.014

[8] N. Soin, P.F. Zhao, K. Prashanthi, J.K. Chen, P. Ding, E.P. Zhou, T. Shab, S.C. Ray, C. Tsonos, T. Thundat, E. Siores, J.K. Luo, High performance triboelectric nanogenerators based on phase-inversion piezoelectric membranes of poly(vinylidene fluoride)-zinc stannate (PVDF-ZnSnO3) and polyamide-6 (PA6), Nano Energy 30 (2016) 470-480. https://doi.org/10.1016/j.nanoen.2016.10.040

[9] L. Xu, T.Z. Bu, X.D. Yang, C. Zhang, Z.L. Wang, Ultrahigh charge density realized by charge pumping at ambient conditions for triboelectric nanogenerators, Nano Energy 49 (2018) 625-633. https://doi.org/10.1016/j.nanoen.2018.05.011

[10] S. Niu, S. Wang, L. Lin, Y. Liu, Y.S. Zhou, Y. Hu, Z.L. Wang, Theoretical study of contact-mode triboelectric nanogenerators as an effective power source, Energ. Environ. Sci. 6(12) (2013) 3576-3583. DOI: 10.1039/C3EE42571A

[11] S.M. Niu, Y. Liu, Y.S. Zhou, S.H. Wang, L. Lin, Z.L. Wang, Optimization of Triboelectric Nanogenerator Charging Systems for Efficient Energy Harvesting and Storage, Ieee. T. Electron. Dev. 62(2) (2015) 641-647. DOI: 10.1109/TED.2014.2377728

[12] B. Yang, W. Zeng, Z.H. Peng, S.R. Liu, K. Chen, X.M. Tao, A Fully Verified Theoretical Analysis of Contact-Mode Triboelectric Nanogenerators as a Wearable

Power Source, Adv. Energy. Mater. 6(16) (2016). https://doi.org/10.1002/aenm.201600505

[13] D. Davies, Charge generation on dielectric surfaces, J. Phys. D. Appl. Phys. 2(11) (1969) 1533. https://doi.org/10.1088/0022-3727/2/11/307

[14] J. Chun, B.U. Ye, J.W. Lee, D. Choi, C.-Y. Kang, S.-W. Kim, Z.L. Wang, J.M. Baik, Boosted output performance of triboelectric nanogenerator via electric double layer effect, Nat. commun. 7 (2016) 12985. https://doi.org/10.1038/ncomms12985

[15] S.R. Liu, W. Zheng, B. Yang, X.M. Tao, Triboelectric Charge Density of Porous and Deformable Fabrics Made from Polymer Fibers, Nano Energy (2018), NANOEN3001. https://doi.org/10.1016/j.nanoen.2018.08.071

[16] J. Chun, J.W. Kim, W.-s. Jung, C.-Y. Kang, S.-W. Kim, Z.L. Wang, J.M. Baik, Mesoporous pores impregnated with Au nanoparticles as effective dielectrics for enhancing triboelectric nanogenerator performance in harsh environments, Energ. Environ. Sci. 8(10) (2015) 3006-3012. DOI: 10.1039/C5EE01705J

[17] S.H. Wang, Y.N. Xie, S.M. Niu, L. Lin, C. Liu, Y.S. Zhou, Z.L. Wang, Maximum Surface Charge Density for Triboelectric Nanogenerators Achieved by Ionized-Air Injection: Methodology and Theoretical Understanding, Adv. Mater. 26(39) (2014) 6720-6728. https://doi.org/10.1002/adma.201402491

[18] Y.P. Raizer, J.E. Allen, Gas discharge physics, Springer Berlin1997.

[19] D.B. Go, D.A. Pohlman, A mathematical model of the modified Paschen's curve for breakdown in microscale gaps, J. Appl. Phys. 107(10) (2010). https://doi.org/10.1063/1.3380855

[20] D.B. Go, A. Venkattraman, Microscale gas breakdown: ion-enhanced field emission and the modified Paschen's curve, J. Phys. D. Appl. Phys. 47(50) (2014). https://doi.org/10.1088/0022-3727/47/50/503001

[21] A. Peschot, N. Bonifaci, O. Lesaint, C. Valadares, C. Poulain, Deviations from the Paschen's law at short gap distances from 100 nm to 10 μm in air and nitrogen, Appl. Phys. Lett. 105(12) (2014). https://doi.org/10.1063/1.4895630

[22] P.G. Slade, E.D. Taylor, Electrical breakdown in atmospheric air between closely

spaced (0.2 mu m-40 mu m) electrical contacts, Ieee. T. Compon. Pack. T. 25(3) (2002) 390-396. DOI: 10.1109/TCAPT.2002.804615

[23] Y.L. Zi, C.S. Wu, W.B. Ding, Z.L. Wang, Maximized Effective Energy Output of Contact-SeparationTriggered Triboelectric Nanogenerators as Limited by Air Breakdown, Adv. Funct. Mater. 27(24) (2017). https://doi.org/10.1002/adfm.201700049

[24] A.N. Ionov, E.O. Popov, A.A. Pashkevich, V.M. Svetlichnyi, M.N. Nikolaeva, Field emission from metal covered by film of polymer insulator, Ivesc2004: The 5th International Vacuum Electron Sources Conference Proceedings (2004) 84-84. DOI: 10.1109/IVESC.2004.1414142

[25] Y.L. Zi, S.M. Niu, J. Wang, Z. Wen, W. Tang, Z.L. Wang, Standards and figure-of-merits for quantifying the performance of triboelectric nanogenerators, Nat. Commun. 6 (2015). https://doi.org/10.1038/ncomms9376

[26] S. Trigwell, N. Grable, C.U. Yurteri, R. Sharma, M.K. Mazumder, Effects of surface properties on the tribocharging characteristics of polymer powder as applied to industrial processes, IEEE Trans. Ind. Appl. 39(1) (2003) 79-86. DOI: 10.1109/TIA.2002.807228

[27] D.K. Davies, M.A. Biondi, Vacuum electrical breakdown between plane-parallel copper electrodes, J. Appl. Phys. 37(8) (1966) 2969-2977. https://doi.org/10.1063/1.1703148

Figures

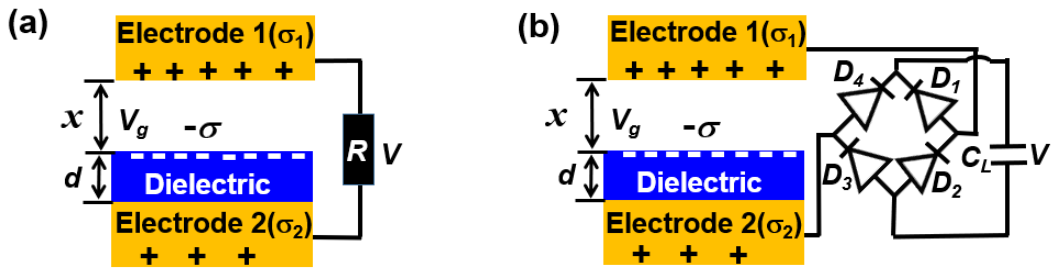

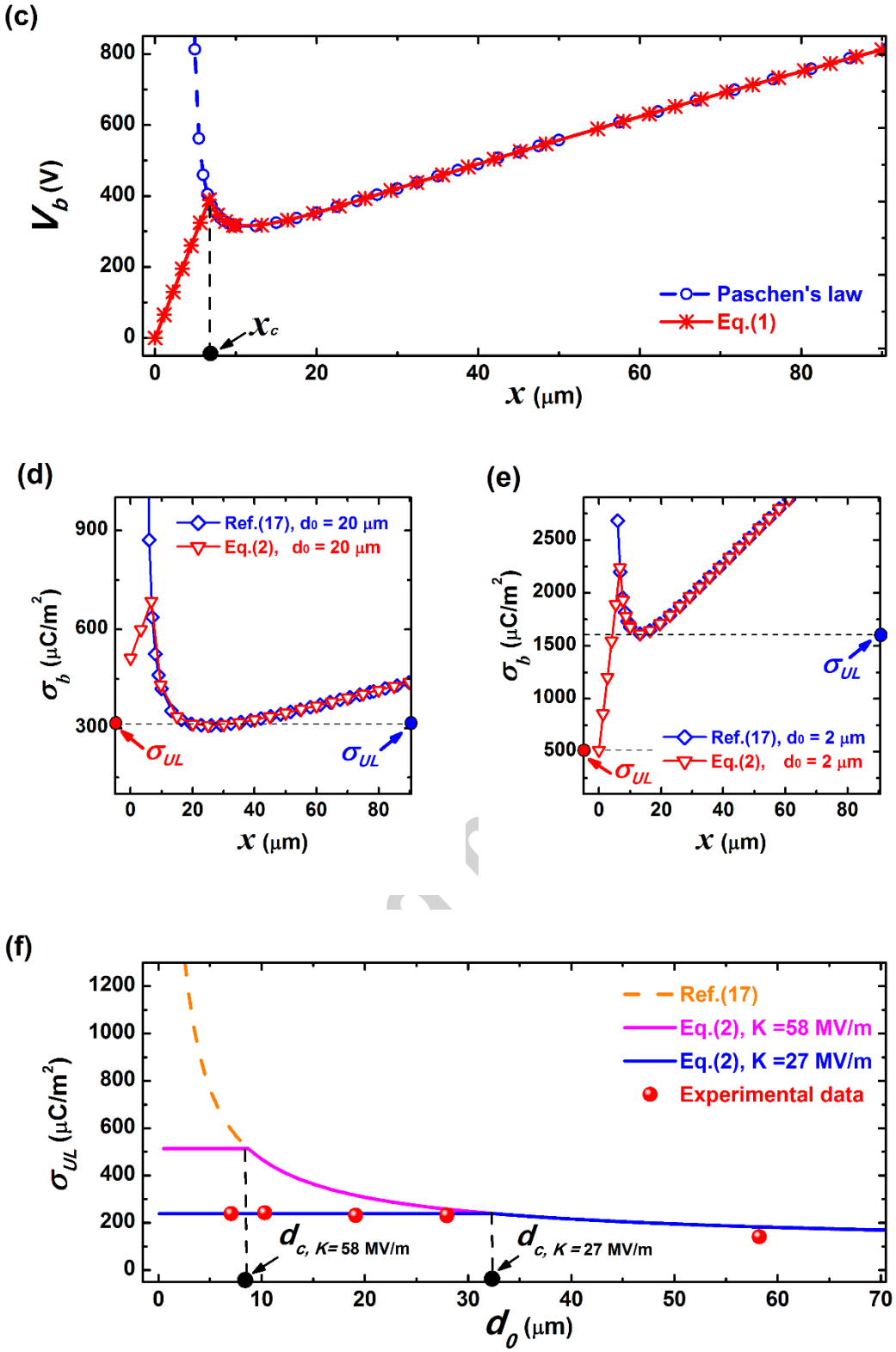
(c)
V_b (V)
x (μm)
x_c
Paschen's law
Eq.(1)
(d)
σ_b (μC/m^2)
Ref.(17), d0 = 20 μm
Eq.(2), d0 = 20 μm
σ_{UL}
x (μm)
(e)
σ_b (μC/m^2)
Ref.(17), d0 = 2 μm
Eq.(2), d0 = 2 μm
σ_{UL}
x (μm)
(f)
σ_{UL} (μC/m^2)
Ref.(17)
Eq.(2), K =58 MV/m
Eq.(2), K =27 MV/m
Experimental data
$d_{c,\ K=58\ MV/m}$
$d_{c,\ K=27\ MV/m}$
d_0 (μm)

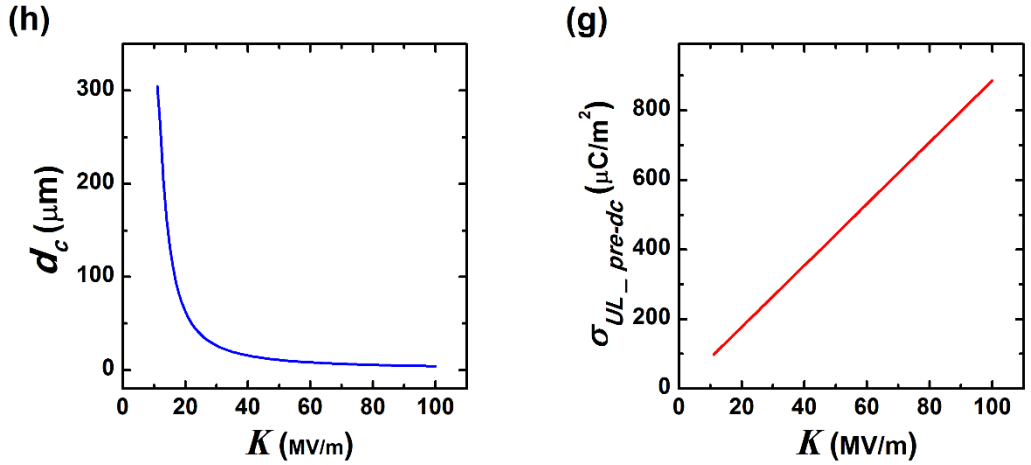

Figure 1. Schematic diagram of a contact-mode TENG connected with external load of (a) an external resistor and (b) an external capacitor with a full-bridge rectifier, respectively; (c) Plots of breakdown voltage of air; (d) and (e) Surface charge density at electric breakdown, σ_b, where two different effective thickness of the dielectric layer, d_0, are illustrated to show the influence of K on the upper limit of surface charge density, σ_{UL}; (f) Theoretical relationship between σ_{UL} and d_0, with the experimentally obtained surface charge density on polydimethylsiloxane (PDMS) for d_0 of 7, 10, 19, 28, and 58 μm, respectively; (g) Relationship between σ_{UL} in pre-d_c region, $\sigma_{UL\_pre\text{-}dc}$, and K, and (h) Relationship between the critical thickness of dielectric layers, d_c, and K.

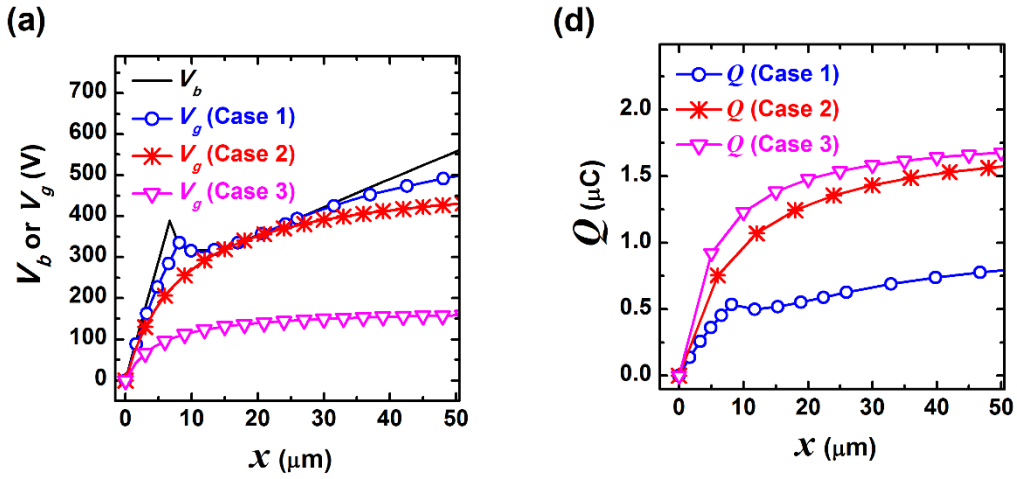

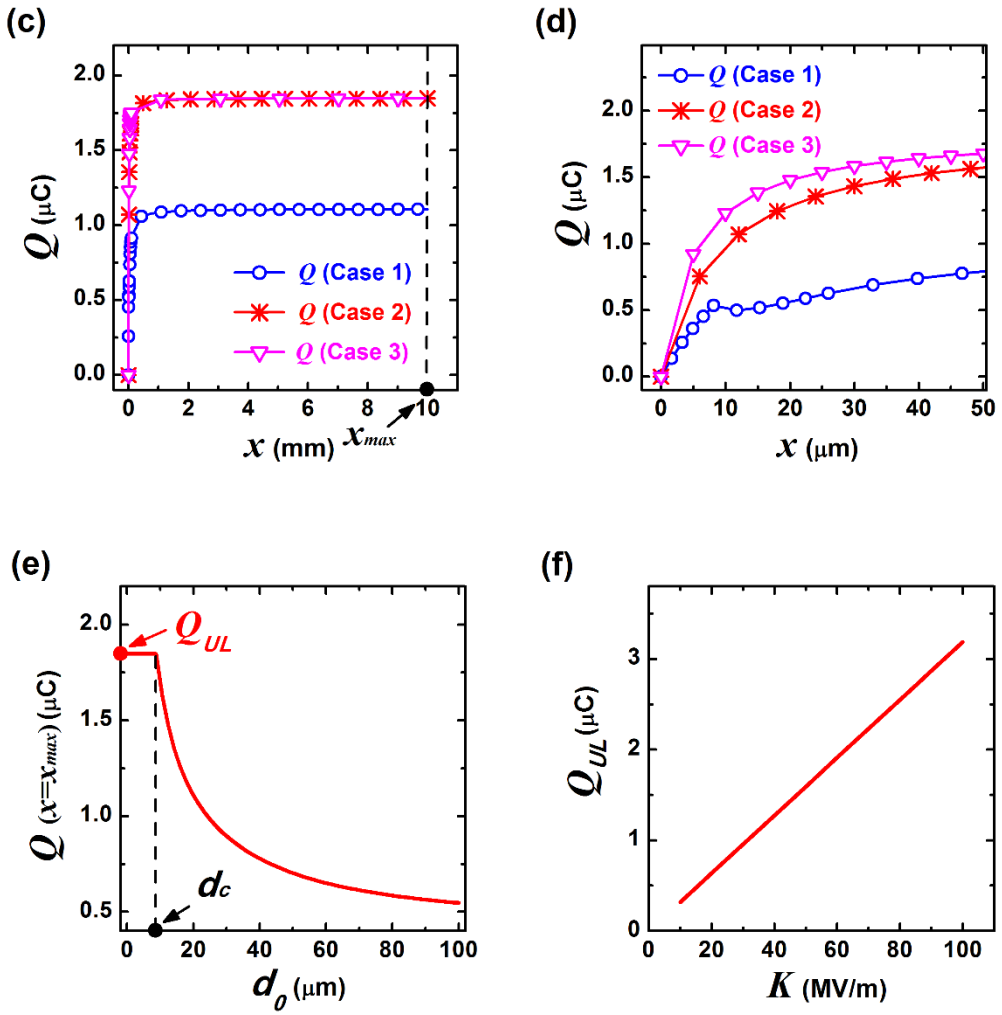

Figure 2. (a) Plot of V_b and V_g for a given TENG under the short-circuit condition, where a rapidly increasing curve of V_g at a large d_0 (20 μm) contacts the part of V_b defined by Paschen's law, marked as cases 1, a slowly increasing curve of V_g at a small d_0 (5 μm) never reaches V_b, marked as cases 3, and between case 1 and case 3, a curve of V_g at a critical value of d_c (8.7 μm) tangentially contacts V_b at one point, marked as case 2; (b) Plot of σ in case 1, 2, and 3, respectively; (c) Plot of the transferred charge, Q, in case 1, 2, and 3, respectively, and (d) enlarged the plots in the range from 0 to 50 μm; (e) Relationship between Q at the max separation distance, x_{max}, and d_0; (f) A linear relationship between the upper limit of transferred charge, Q_{UL}, and K.

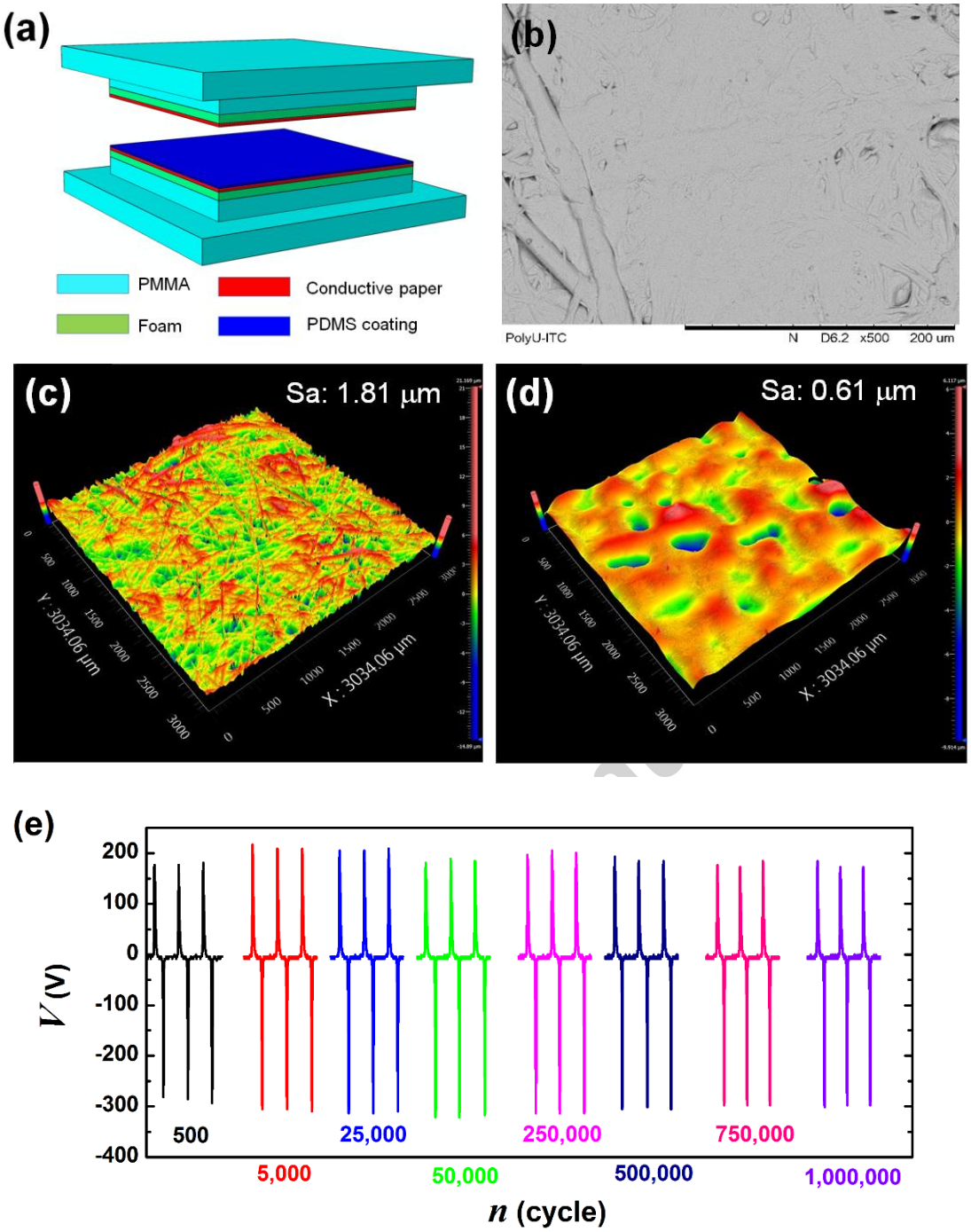

Figure 3 (a) Schematic diagram of a laboratory-fabricated TENG, (b) SEM of Cu/Ni coated aramid paper, (c) Surface profile of Cu/Ni coated aramid paper (thickness of 63 μm), (d) Exampled surface profile of PDMS coating (d_0 of 28 μm), and (e) Output voltage across a resistor of 8 MΩ from the fabricated TENG working system, where Cu/Ni coated aramid paper (thickness of 63 μm), PDMS coating (d_0 of 28 μm), polymer foam (thickness of 2 mm) are in use, a sinusoidal motion with max separation distance of 10 mm, peak pressure of 278 kPa, and frequency of about 3 Hz is applied.

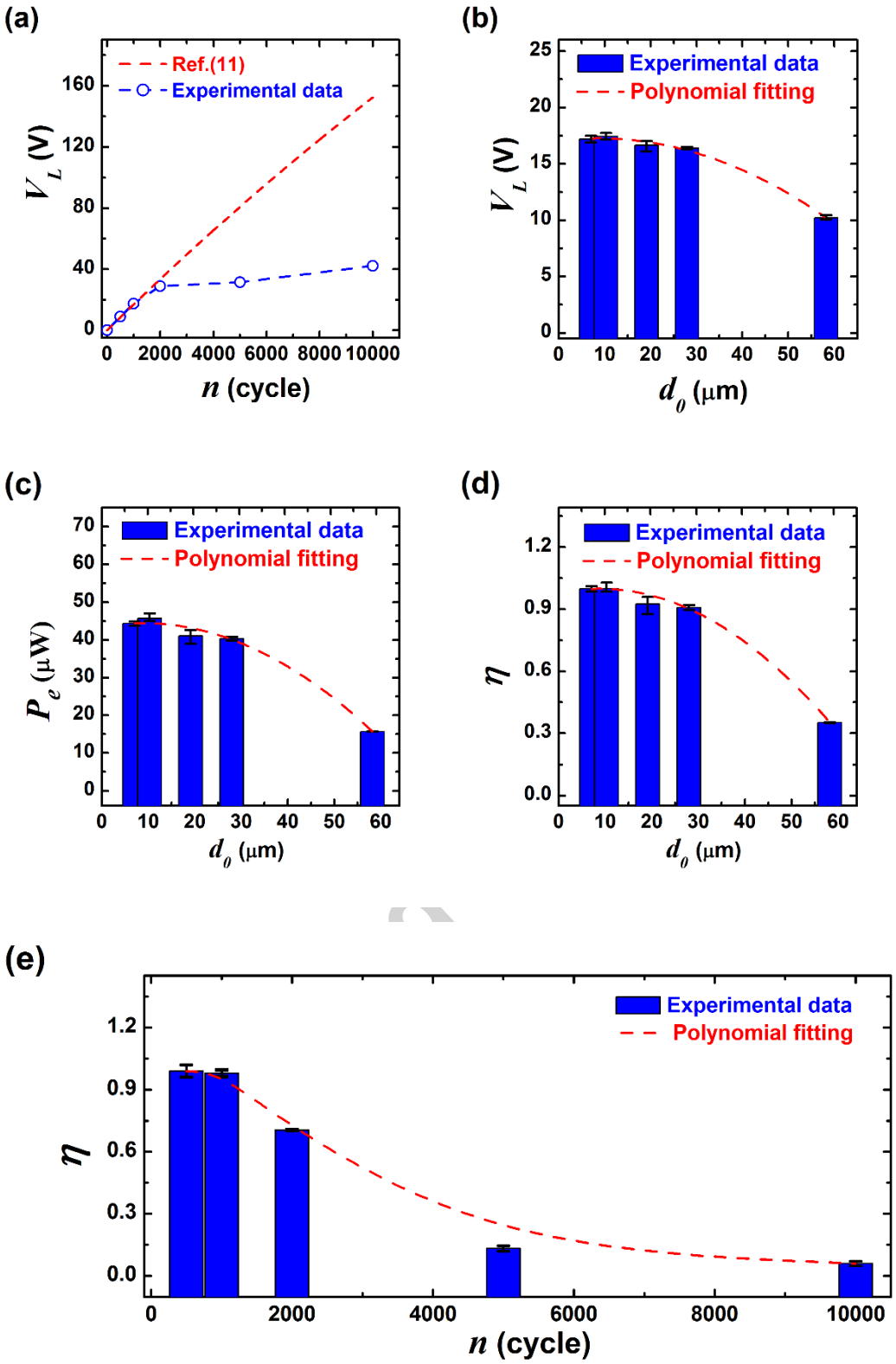

Figure 4 Output performance of a laboratory-fabricated TENG harvesting system (shown in Figure 1b and 3a): (a) Relationship between the compression cycle, n, and the harvesting voltage, V_L, across the external capacitor (100 μF), where d_0 of PDMS coating is 28 μm; (b) V_L after 1000 cycle, with five different thickness, d_0, of 7, 10, 19, 28 and 58 μm, and (c) Corresponding output power; (d) Working efficiency, η, of the

fabricated TENG harvesting system with different thickness of d_0 at 1000 cycles, and (e) η of the fabricated TENG harvesting system with compression cycle of n (corresponding to (a)); where other parameters is given below: Cu/Ni coated aramid paper (thickness of 63 μm), polymer foam (thickness of 2 mm), a sinusoidal motion with max separation distance of 10 mm, peak pressure of 278 kPa, and frequency of about 3 Hz.

Table 1 Parameters utilized in calculation

Symbol	**Value**
Constant, A [18]	10.95 Pa/m
Constant, B [18]	273.78 V/Pa/m
Gas pressure, p [18]	101325 Pa
Secondary ionization coefficient, γ [19]	0.01
Threshold electric field, K [19]	58 MV/m
Area size, S	36 cm^2
Frequency, f	3 Hz
Effective thickness of dielectric, d_0	20 μm
Max separation distance, x_{max}	10 mm
Initial phase angle, θ_0	3π/2
External capacitance, C_L	100 μF
Vacuum permittivity, ε_0	8.85×10^{-12} F/m
Number of cycles, n	1 000 cycles

Highlights

- Based on mechanisms of field emission from cathodes and gas -ionization for electric breakdown, new theoretical models of contact-mode triboelectric nanogenerator harvesting systems to predict their upper limits of surface charge density, transferred charge, and possessing output power.
- Constant surface charge density on the dielectric layer, with a small effective

thickness below a critical thickness of d_c, and resultant high output power of such a TENG.

- Power tools to guide in selection of materials, design of device structures and harvesting circuits.